

Nanostructure of Calcium Silicate Hydrates in Cements

L. B. Skinner,¹ S. R. Chae,¹ C. J. Benmore,² H. R. Wenk,³ and P. J. M. Monteiro^{1,*}

¹*Department of Civil and Environmental Engineering, University of California, Berkeley, California 94720, USA*

²*Advanced Photon Source, Argonne National Laboratory, 9700 South Cass Avenue, Argonne, Illinois 60439, USA*

³*Department of Earth and Planetary Science, University of California, California 94720, USA*

(Received 4 February 2010; published 11 May 2010)

Calcium silicate hydrate (CSH) is the major volume phase in the matrix of Portland cement concrete. Total x-ray scattering measurements with synchrotron x rays on synthetic CSH(I) shows nanocrystalline ordering with a particle diameter of 3.5(5) nm, similar to a size-broadened 1.1 nm tobermorite crystal structure. The CSH component in hydrated tricalcium silicate is found to be similar to CSH(I). Only a slight bend and additional disorder within the CaO sheets is required to explain its nanocrystalline structure.

DOI: [10.1103/PhysRevLett.104.195502](https://doi.org/10.1103/PhysRevLett.104.195502)

PACS numbers: 61.05.cf

Although calcium silicate hydrate (CSH) is critical to cement paste strength and durability, many ambiguities remain regarding its atomic structure. This knowledge is vital for optimizing CSH-based concretes with the aim of reducing the CO₂ associated with its production. Despite extensive study, CSH in cements has continued to escape detailed and direct atomic structure analysis for two main reasons: difficulty in separating it from other phases and its broad diffraction signal. The manufacture of every ton of Portland clinker emits approximately 0.8 tons of CO₂ into the atmosphere, comprising 5%–7% of the total human-made CO₂ emission. CSH is the main binding phase in a Portland cement matrix; therefore, there is strong motivation to optimize the strength and durability of CSH so that less cement is used. Despite the vast amount of literature available on cementitious materials, many questions and ambiguities on the understanding of the atomic scale structure of this cement remain.

Colloidal models proposed by Jennings [1,2] elegantly explain several bulk properties of CSH found in hydrated cement pastes. The basis of these models is the existence of a <5 nm diameter building block in CSH. Although neutron scattering [2], electron microscopy [3], and computer simulation [4] have suggested the existence of such nanograins, they have yet to be demonstrated beyond reasonable doubt. For example, one currently unsolved question is: If they exist, why do these nanograins not grow larger? An improved understanding of the atomic arrangement in cement paste can provide a basis for intelligently designing concrete with enhanced properties because one can manipulate the layered CSH structure and create a true hybrid CSH with such detailed structural information. For example, organic polymeric additives have shown to strongly interact with the surface of hydrated CSH [5], yet controlling the exact pathways or mechanism of the interaction between the organic molecules and CSH is limited to date mainly due to the limitation on the knowledge of the precise structure of CSH.

Because of a lack of conclusive data, there have been many different structural models suggested for CSH [6]. Most of the currently accepted models use the following structural basis: riversideite (0.9 nm tobermorite), tobermorite (1.1 nm), plombierite (1.4 nm tobermorite), and jennite crystal structures. Tobermorite minerals, which have an atomic Ca/Si ratio in the range 0.75–1 are close in composition to the synthetic CSH(I) Ca_{0.13}Si_{0.13}O_{0.51}H_{0.23} studied in this work. Since the work of Taylor [7], the general consensus has been that CSH(I) with Ca/Si ratio <1 is a disordered form of 1.4 nm tobermorite. Current solid solution models explain the compositional differences, especially at high Ca/Si ratio CSH, with the combination with jennite (which itself has a Ca/Si = 1.5) and Ca(OH)₂ structures [8]. The application of pair distribution function (PDF) techniques [9]—not previously applied to CSH—aim to test and improve the existing structural models. In the research described below, measurements were conducted on synthetic CSH(I) and hydrated tricalcium silicate paste (hyd-C3S). The synthetic CSH(I) has the advantage that it is free of the crystalline Ca(OH)₂ and Ca₃SiO₅ phases present in hyd-C3S. The hyd-C3S sample represents real cement pastes as it is the same hydration of calcium silicates through which CSH with a high Ca/Si ratio is formed in cement pastes.

X-ray diffraction measurements were made at the advanced photon source, beam line 11-ID-C at Argonne National Laboratory. The experimental details and analysis procedures are given in [10]. The x-ray structure function for synthetic CSH (I) and hyd-C3S are shown in Fig. 1 together with glassy (Si + Al)_{0.26}Ca_{0.16}O_{0.58} from [11]. Although the CSH pattern is very different compared to the nonhydrated glass, it does not contain any sharp Bragg peaks like those present in the hydrated tricalcium silicate paste (hyd-C3S). From this we conclude that the synthetic CSH(I) is not truly amorphous and does not contain any large well ordered crystals. Consequently, the well-defined tobermoritelike infinite CaO sheets

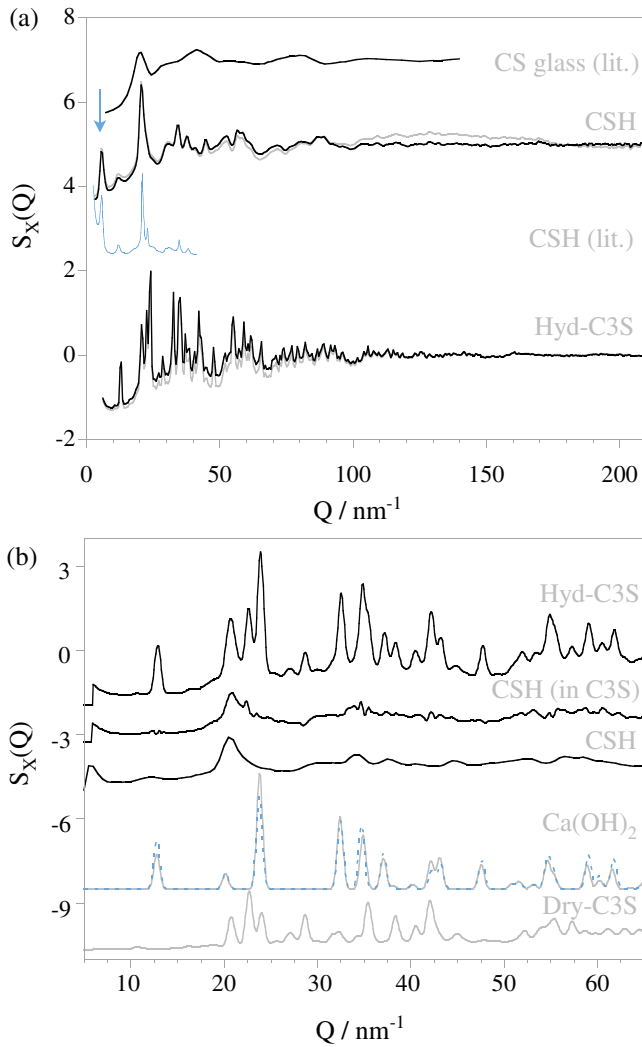


FIG. 1 (color). (a) X-ray structure factors $S_X(Q)$ of synthetic $\text{Ca}_{0.13}\text{Si}_{0.13}\text{O}_{0.51}\text{H}_{0.23}$ (CSH, middle) and hydrated Ca_3SiO_5 (hyd-C3S, bottom). A similar composition nonhydrated Ca-Si-O glass from [11] (top). The (light) grey lines are the raw data, and (dark) black lines are the back transforms after removal of $r < 0.1$ nm features [10]. The blue line labeled CSH (lit.) from Ref [12], represents CSH with $\text{Ca}/\text{Si} = 0.8$. The arrow indicates the 1.1 nm d -spacing position of the basal peak in both the CSH patterns. (b) The measured diffraction patterns of hydrated C_3S paste (top), and the isolated CSH component (2nd top) after subtraction of the crystalline components (lower patterns). The (light) grey $\text{Ca}(\text{OH})_2$ pattern is taken from [19], whereas the blue dotted $\text{Ca}(\text{OH})_2$ pattern has been refined to eliminate Bragg peaks in the remaining CSH (in C3S) pattern [10]. Also plotted is the synthetic CSH(I) pattern (scaled by 0.65) for comparison.

and SiO chains, if present, must be either short or disordered.

The hyd-C3S sample is a combination of three components: unreacted crystalline Ca_3SiO_5 , $\text{Ca}(\text{OH})_2$ crystals, and CSH. To isolate the CSH x-ray scattering pattern, Ca_3SiO_5 and $\text{Ca}(\text{OH})_2$ need to be subtracted from the

bulk pattern. The resulting function shows agreement between the synthetic CSH measurement and the CSH component of the hyd-C3S [10]. The position of the low- Q (basal) peak in the synthetic CSH(I) is centered at a d spacing of 1.1(1) nm, contrary to the often used 1.4 nm tobermorite crystal structure. This confirms previous observations [8], although examples of higher basal spacings have also been reported [5]. The broadened 1.1 nm tobermorite model in Fig. 2 is similar to the measured synthetic CSH(I) spectrum, contrary to the broadened 1.4 nm tobermorite model [8]. From this we conclude that the structure of the synthetic CSH(I) resembles 1.1 nm tobermorite.

Although similar in their CaO_7 sheet and SiO_4 chain substructure, the crystal structures used for 1.1 and 1.4 nm tobermorite differ in the alignment of adjacent layers and the partial occupancies of Ca and water in the interlayer regions, as well as the layer spacing itself (see Fig. 2). Another important observation from the comparisons in Fig. 2 is that the broadened tobermorite patterns represent perfectly ordered, very small crystals. In other words, the synthetic CSH(I) structure is remarkably similar to that expected for randomly packed small 1.1 nm tobermorite crystallites [13].

Figure 3 shows a detailed comparison of the measured CSH(I) PDF, and that of 1.1 nm tobermorite. The tetrahedral coordination is further confirmed by the symmetry and position (0.162 nm) of the SiO peak. Similarly, the area and position of the peak at 0.24(1) nm confirm that the presence of CaO_7 polyhedra on average in CSH(I). The tobermorite crystal partial structure factors were combined with the synthetic CSH(I) x-ray weighting factors and Fourier trans-

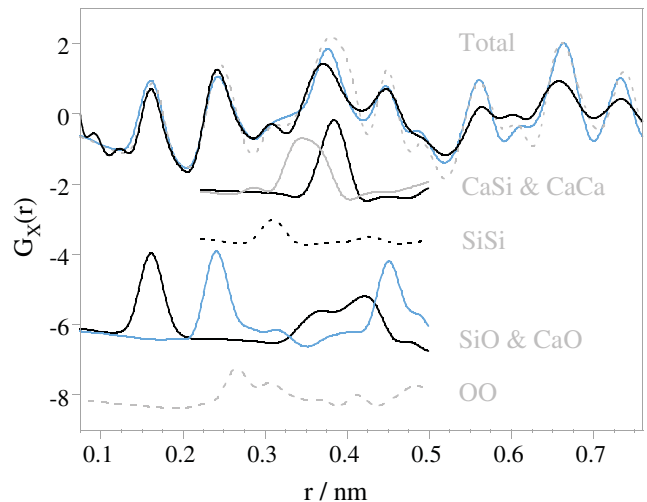


FIG. 2 (color). The measured $G_X(r)$ (black line, top) and the equivalently weighted $G_X(r)$ from the Hamid [16] and Merlino *et al.* [17] crystal structures (blue and grey dotted top lines, respectively). Also shown is the x-ray weighted partial structure factors for the Hamid structure. From top to bottom Grey = CaSi, Black = CaCa, Black dotted = SiSi, Black = SiO, blue = CaO, grey dotted = OO.

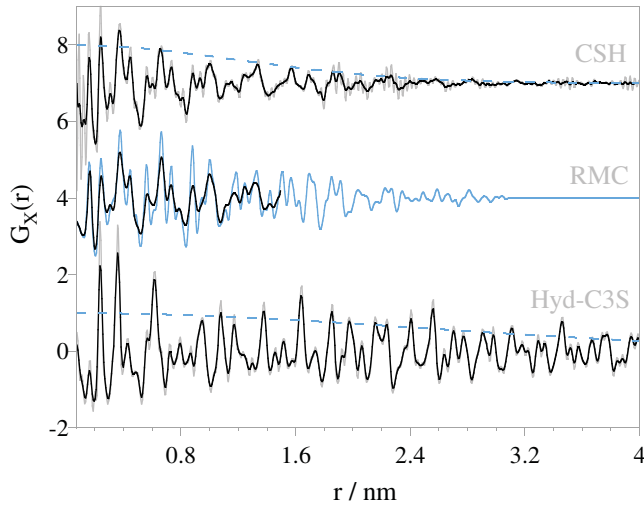


FIG. 3 (color). The x-ray pair distribution functions of synthetic CSH(I) (top black line, obtained using a Lorch modification function, light grey is the raw transform) and hyd-C3S (lower black and grey lines). The lower dashed blue line shows the intensity damping present due to the finite Q resolution, whereas the upper dashed line approximates the damping present in the CSH(I) sample due to grain size. The middle curves are the distribution functions of 1.1 nm tobermorite before and after refinement to fit the measured data.

formed over the same Q range as the measured data. Isotropic thermal broadening parameters of each atom type were refined to match the width of the SiO and CaO peaks. The nearest neighbor environment in CSH(I) and 1.1 nm tobermorite are very similar. The second neighbor CaO peak at 0.4–5 nm is a signature of the CaO sheet structure, which must also be present in the CSH(I) sample. The small peak around 0.3 nm is consistent with corner-shared tetrahedra forming Si-O-Si bonds. The largest difference between the crystal and CSH(I) is in the CaCa/CaSi nearest neighbor correlations. To match the CSH(I) measurement the Ca-Ca separation must be broadened and shortened by 0.003–0.01 nm relative to the tobermorite crystal structure. This implies a slight bending of the Ca-O sheet, which may account for the limited size of the nanocrystalline particles.

Features in the CSH(I) measurement at length scales longer than the nearest neighbor become strongly damped relative to the crystal (see Fig. 3). This damping is well explained by nanocrystalline grain size damping the structural coherence. The damping in real space corresponds directly to broadening of features in Q space and is differentiated from more specific local structural disorder (bending of sheets, chains, or distortion of polyhedra) that would be present as distortion of peaks in the real space pattern. Here it is clear the CSH(I) has no correlated structure past 3.5 nm. Although the loss of structural coherence itself is not evidence of nanocrystallinity, a strong argument can be made to suggest nanograins of

this size, based on the similarity of the PDF of CSH and the size-broadened crystal structures and on small angle neutron scattering [2]. The presence of nanocrystalline regions in CSH was also observed in a comprehensive characterization by high resolution transmission electron microscopy that reported crystalline regions of about 5 nm, with local structural ordering corresponding to tobermorite [14,15]. The transmission electron microscopy experiments on selected areas [14,15] show considerable Ca:Si ratio fluctuations, homogeneous nanocrystalline regions, and document that CSH possesses short-range order. Building on this, our PDF measurements provide a means of quantitatively modelling the average atomic distributions of the nanocrystalline CSH structure not accessible using other techniques.

Plotted in Fig. 3 is a reverse Monte Carlo refinement of the tobermorite crystal structure. Here, once damping due to nanocrystallinity is fully accounted for, little disorder within the nanograin is required to explain the broad diffraction patterns. The basic difference between the 1.1 nm Hamid-type structure [16] and the Merlino 1.1 nm type structure [17] is that the former structure has misaligned and separated Si-O chains while in the latter structure one-third of the tetrahedra are Q^3 (connecting adjacent chains). Our PDF results are not able to quantify the Q^3 speciation or distinguish conclusively between these two models, so for simplicity only the results for the Hamid's structure are reported. The unit cell of 1.1 nm tobermorite has dimensions $0.67 \times 0.74 \times 2.27$ nm, with a unit cell volume = 0.940 nm³. A spherical nanocrystal with a 3.5 nm diameter has a volume of roughly 24 unit cells; i.e., each dimension is 2–5 unit cells across. This partially explains the short chain lengths observed for CSH. Data from [18] for CSH(I) (samples with Ca/Si = 1 ± 0.15) give mean chain lengths in the range 3–6. This is a length of 0.7–1.5 nm, meaning only 1–2 (out of 5) bridging tetrahedra per chain, within a nanograin need be disconnected. Hence nanocrystallinity offers a good explanation as to why the silicate chains are so short in CSH.

Diffraction measurements obtained in this research agree with previous measurements (see [8,18]) that show the CSH system to be much more crystalline in structure than typical liquids or glasses. Here, the CSH(I) structure was found to be remarkably close to a size-broadened version of Hamid's 1.1 nm tobermorite. In real space, the pair distribution function was found to be structureless past 3.5(5) nm. Given the results obtained here it can be concluded that CSH is nanocrystalline. After compensating for nanocrystallinity, structures with a relatively high degree of order within the nanocrystals are found to be consistent with the experimental data. This result is novel. Molecular dynamics techniques are also providing new structural information on CSH [4,19], but generally contain much more disorder within these nanograins than we observe. Consequently, our data will improve the understanding

of the CSH structure for the investigation and improvement of engineering the hybrid CSH structure with enhanced cementitious properties. The methodology described here can also be used to determine the modifications produced in the CSH as high percentages of industrial waste such as fly ash and slag are used to produce environmentally correct concrete.

This publication was based on work supported in part by Grant No. KUS-11-004021, made by King Abdullah University of Science and Technology (KAUST). This work was supported by the U.S. DOE, Argonne National Laboratory under Contract No. DE-AC02-06CH11357. Also, thanks to Dr. Simon Clark, Dr. Juyoung Ha, Cagla Meral, and Elizabeth Mannering for their help with the production of this paper; and to Gordon Chan and Dr. Laila Raki for their help with the sample synthesis.

*Corresponding author.

monteiro@ce.berkeley.edu

- [1] H. M. Jennings, *Cement and Concrete Research* **38**, 275 (2008).
- [2] A. Allen, J. J. Thomas, and H. M. Jennings, *Nature Mater.* **6**, 311 (2007).
- [3] X. Zhang, W. Chang, T. Zhang, and C. K. Ong, *J. Am. Ceram. Soc.* **83**, 2600 (2000).
- [4] H. Manzano, A. Ayuela, and J. S. Dolado, *J. Comput.-Aided Mater. Des.* **14**, 45 (2007).
- [5] A. Popova and G. Geoffroy, *J. Am. Ceram. Soc.* **83**, 2556 (2000).
- [6] I. G. Richardson, *Cement and Concrete Research* **38**, 137 (2008).
- [7] H. F. W. Taylor, *J. Am. Ceram. Soc.* **69**, 464 (1986).
- [8] R. Alizadeh, J. J. Beaudoin, and L. Raki, *J. Am. Ceram. Soc.* **90**, 670 (2007).
- [9] S. J. L. Billinge and I. Levin, *Science* **316**, 561 (2007).
- [10] See EPAPS Document No. <http://link.aps.org/supplemental/10.1103/PhysRevLett.104.195502> for analysis details.
- [11] L. Cormier, *J. Am. Ceram. Soc.* **88**, 2292 (2005).
- [12] H. Matsuyama and J. F. Young, *J. Mater. Res.* **14**, 3379 (1999).
- [13] A. Nonat, *Cement and Concrete Research* **34**, 1521 (2004).
- [14] Z. Xu and D. Viehland, *Phys. Rev. Lett.* **77**, 952 (1996).
- [15] D. Viehland, J. F. Li, L. J. Yuan, and Z. Xu, *J. Am. Ceram. Soc.* **79**, 1731 (1996).
- [16] S. A. Hamid, *Z. Kristallogr.* **154**, 189 (1981).
- [17] S. Merlino, E. Bonaccorsi, and T. Armbruster, *Eur. J. Mineral.* **13**, 577 (2001).
- [18] X. Cong and R. J. Kirkpatrick, *Advanced Cement Based Materials (1993-): ACBM* **3**, 144 (1996).
- [19] R. J. M. Pellenq *et al.*, *Proc. Natl. Acad. Sci. U.S.A.* **106**, 16102 (2009).